Chalcogen-Assisted Enhanced Atomic Orbital Interaction at TMD–Metal Interface and Sulfur Passivation for Overall Performance Boost of 2-D TMD FETs

Ansh, Jeevesh Kumar, Gaurav Sheoran, Harsha B. Variar, Ravikesh Mishra, Hemanjaneyulu Kuruva, Adil Meersha, Abhishek Mishra, Srinivasan Raghavan, and Mayank Shrivastava, *Senior Member, IEEE*

***Abstract*— Metal–semiconductor interface is a bottleneck for the efficient transport of charge carriers through transition metal dichalcogenide (TMD)-based FETs. Injection of charge carriers across such interfaces is mostly limited by the Schottky barrier at the contacts that must be reduced to achieve highly efficient contacts for carrier injection into the channel. Here, we introduce a universal approach involving dry chemistry to enhance atomic orbital interaction among various TMDs (MoS_2, WS_2, $MoSe_2$, and WSe_2) and metal contacts. Quantum chemistry among TMDs, chalcogens, and metals has been explored using detailed atomistic (DFT and NEGF) simulations, which is then verified using Raman, PL, and XPS investigations. Atomistic investigations revealed lower contact resistance due to the enhanced orbital interaction and unique physics of charge sharing between constituent atoms in TMDs with the introduced chalcogen atoms that are subsequently validated through experiments. In addition to contact engineering, which resulted in contact resistance (extracted via the Y-function method as low as 119 and 59 $\Omega\mu$m in MoS_2 and WS_2, respectively), a novel approach to cure/passivate the dangling bonds present at the 2-D TMD channel surface has been demonstrated. While the contact engineering improved the ON-state performance (I_{ON}, g_m, μ, and R_{ON}) of the 2-D TMD FETs by orders of magnitude, chalcogen-based channel passivation was found to improve gate control (I_{OFF}, SS, and V_{TH}) significantly. This resulted in an overall performance boost. The engineered TMD FETs were shown to have performance on par with the best reported until now.**

***Index Terms*— Atomic orbital interaction, MoS_2, $MoSe_2$, transition metal dichalcogenides (TMDs), WS_2, WSe_2.**

Manuscript received October 17, 2019; revised November 23, 2019; accepted December 2, 2019. Date of publication January 10, 2020; date of current version January 27, 2020. This work was supported by the Nanoelectronics Network for Research and Applications (NNetRA) Program of Ministry of Electronics and Information Technology (MeitY), Department of Science and Technology (DST) and the Ministry of Human Resource Development (MHRD), Government of India. The review of this article was arranged by Editor G. L. Snider. *(Corresponding author: Ansh.)*

Ansh, J. Kumar, G. Sheoran, H. B. Variar, H. Kuruva, A. Meersha, A. Mishra, and M. Shrivastava are with the Advanced Nanoelectronics Device and Circuit Research Laboratory, Department of Electronic Systems Engineering, Indian Institute of Science, Bengaluru 560012, India (e-mail: ansh@iisc.ac.in; mayank@iisc.ac.in).

R. Mishra and S. Raghavan are with the Centre for Nano Science and Engineering, Indian Institute of Science, Bengaluru 560012, India.

Color versions of one or more of the figures in this article are available online at http://ieeexplore.ieee.org.

Digital Object Identifier 10.1109/TED.2019.2958338

I. Introduction

GROWTH of semiconductor industry is driven by the Moores law, which intends to improve the efficiency of the electronic gadgets in terms of speed and compactness by 2×, every 1.5 years. This is achieved by the aggressive channel length scaling of silicon MOSFETs. On the other hand, channel length scaling leads to short-channel effects (SCEs) like drain-induced source barrier lowering and threshold voltage rolloff due to compromised gate control over channel. This results into higher source-to-drain leakage current, higher subthreshold slope, and lower noise margins, which eventually increases the static power loss across the VLSI system. To mitigate SCE, devices like FinFETs, multi-gate FET, ultrathin body (UTB) FETs [1], [2], and TFETs [3], [4] have been proposed, which offer improved gate control and better SCE immunity. The key in most of the ultrascaled FET concepts is to reduce the channel thickness as the channel length is scaled down. However, scaling channel thickness beyond 5-nm leads to mobility degradation and threshold voltage instability due to quantum confinement and surface dangling bonds, which leads to performance rolloff. Atomically, the thin layers of 2-D semiconductors like transition metal dichalcogenides (TMDs) on the other hand offer better gate control due to the lack of dangling bonds perpendicular to their basal plane as well as missing quantum issues when compared with the bulk semiconductors. This makes 2-D TMDs promising candidates for short-channel FETs [5]. While a decent amount of work has been reported by various authors on improving the performance of 2-D TMDs like MoS_2 [6], $MoSe_2$ [7], [8], WS_2 [9], [10], and WSe_2 [11], [12], they still suffer from high contact resistance, low ON-state current, depletion-mode operation, and poor subthreshold slope. Techniques reported earlier to improve device performance were often parameter-specific, and while they resulted in striking improvement in the target parameter, the overall transistor behavior was often compromised, or the technique fails to offer a scalable process. For example, in earlier works, techniques like doping by potassium [13], PEI [14],chloride ion [15], benzyl viologen [16], methanol [17], tetracyanoquinodimethane (TCNQ) [18], potassium iodide [19], phase engineering [20] on MoS_2, and/or WS_2 have been used to improve the ON-state current. These

methods, however, suffered from one or the other limitations like nonscalability, involvement of wet chemistry, or deterioration of other figure of merit parameters. For instance, scandium contacts have resulted in recording high ON-currents in MoS_2 [21], however at the cost of significant increase in OFF current. In addition, scandium is a highly unstable metal, which is not suitable for the scalable large-scale process. Therefore, it would not be an exaggeration to say that the absence of a scalable or CMOS equivalent process to boost the overall device behavior is a key bottleneck in the development of the 2-D TMD device technology. In this article, we present a scalable and universal method to improve the contact as well as channel properties of 2-D TMD FETs. Based on fundamental insights into the quantum chemistry of the TMD/metal contacts and the mechanism of molecular decomposition of the chalcogen precursor at low temperature, we introduce a H_2S-based dry chemistry to offer better contact and channel properties for a range of TMDs. While there are several wet processes reported earlier by various groups [13]–[20], which do improve the ON-state performance and contact resistance, this is the first proposal on a dry treatment. The proposed H_2S treatment is scalable to the industry scale process. Moreover, it id consistent, and due to its dry nature, is less prone to variability and instability issues, which are commonly seen in wet treatments.

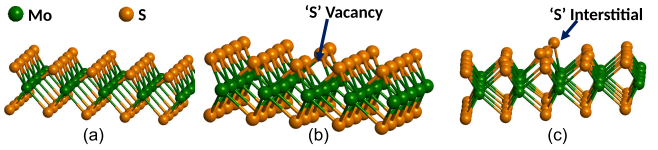

Fig. 1. Optimized structure of 551 super cell of MoS_2. (a) Intrinsic MoS_2. (b) MoS_2 with one "S" vacancy. (c) MoS_2 with "S" at the interstitial site. Similar structures were optimized for all other TMDs.

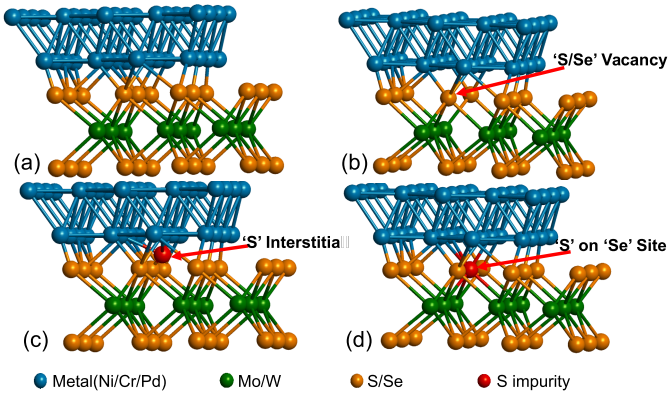

Fig. 2. TMD–metal interface in following configurations. (a) Intrinsic/no defect. (b) TMD with one S or Se vacancy. (c) TMD with S at the interstitial site. (d) TMD with S at Se site.

II. Computational Framework and Simulation Details

A. Band Structure and Density of States (DOS) Calculations

The DFT simulation is done for three different structures of the MoS_2/WS_2 to validate the results. For *ab initio* simulation, the Quantum Wise ATK simulation package has been used. The DFT calculation is performed on a 5×5 MoS_2/WS_2 supercell with single sulfur vacancy, and sulfur on the interstitial site and on the perfect crystal. The local density approximation (LDA) is used as the exchange correlation with 10k points sampling in the periodic directions. 20Å of vacuum space is added at both sides of the atomic plane to eliminate the interplanar wave-function interaction. Before band structure and DOS calculations, all the structures were optimized with 0.01 eV/Å force tolerance and 0.001 eV/Å^3 stress tolerance.

B. Transport Calculations

The metal–semiconductor contacts are created using the Virtual Nano Lab builder in ATK. All the metals were cleaved in the [111] direction before creating the metal–TMDs interfaces to minimize the interface strain. The interface strain is applied on the metal to minimize the strain effect on the TMDs. The extended Hückel semiempirical method of Atomistix ToolKit and NEGF are used for the calculations. The density mesh cutoff is 45 Hartee with 10k points along the width and 200k points along the channel of the devices. Different Hückel basis sets are used for different devices along with a multigrid Poisson solver with the Dirichlet boundary condition. A source–drain bias of 250 mV is applied to conduct the carrier transport analysis on 300 K electron temperature.

C. Various Interface Topologies

The DFT-based band structure and DOS calculations for TMDs (MoS_2, WS_2, $MoSe_2$, and WSe_2) were performed using the Quantum Wise ATK package. A $5 \times 5 \times 1$ supercell of TMD (monolayer) in the following three configurations was studied: 1) intrinsic TMDs [see Fig. 1(a)]; 2) TMDs with one "S" vacancy (for MoS_2 and WS_2) or "Se" vacancy (for $MoSe_2$ and WSe_2) [see Fig. 1(b)]; and 3) TMDs with "S" at the interstitial site of all the TMDs [see Fig. 1(c)]. Transport calculations were performed for the following interface and defect combinations: 1) intrinsic metal–TMD (MoS_2 and WS_2, $MoSe_2$, and WSe_2) interface [see Fig. 2(a)]; 2) metal–TMD interface with "S" (for MoS_2 and WS_2) or Se vacancy (for $MoSe_2$ and WSe_2) [see Fig. 2(b)]; 3) metal–TMD interface with "S" at the interstitial site of all the TMDs [see Fig. 2(c)]; 4) metal–TMD interface with "Se" at the interstitial site (for $MoSe_2$ and WSe_2) [similar to Fig. 2(c)]; and 5) metal–TMD ($MoSe_2$ and WSe_2) interface with one "Se" replaced by "S" at the interstitial site [see Fig. 2(d)].

III. Quantum Chemistry of TMD/Metal Contacts

To begin with, the impact of chalcogen atom at the interstitial sites between the TMD–metal interface, for various material systems—MoS_2/Ni, $MoSe_2$/Ni, WS_2/Cr, and WSe_2/Ni, was studied using the following three contact topologies: 1) defect-free interface; 2) defected (with chalcogen-vacancy) interface; and 3) metal-doped (with chalcogen atom at the interstitial site) interface. It is observed [see Figs. 3 and 4]

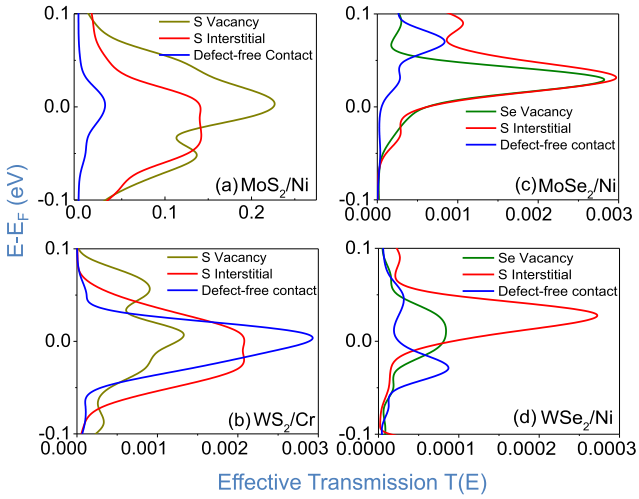

Fig. 3. Effective transmission spectrum T(E) for various 2-D TMD/metal interfaces with varying contact topology. (a) MoS_2/Ni, (b) $MoSe_2$/Ni, (c) WS_2/Cr, and (d) WSe_2/Ni are calculated using the extended Hückel semiempirical method. Higher transmission peak near Fermi level together with wider spread across energy states is observed in the presence of chalcogen interstitial/defect, when compared with standard contacts for all the interfaces. The extent of improvement was, however, found to be independent of the TMD-Metal system.

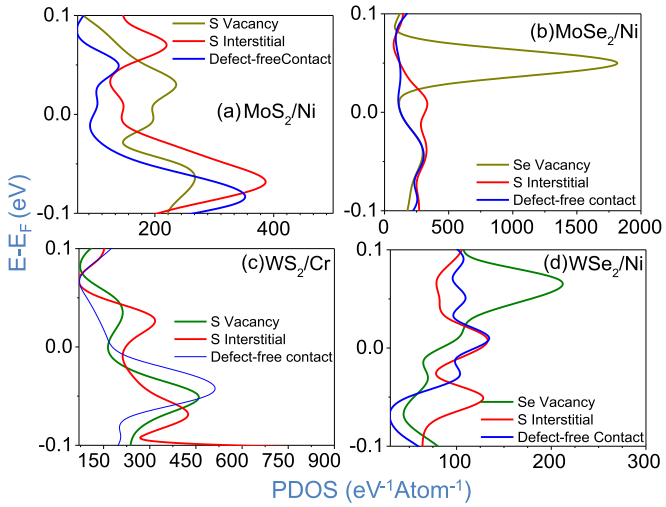

Fig. 4. Partial DOS (PDOS) using different 2-D TMD/metal interfaces. (a) MoS_2/Ni, (b) $MoSe_2$/Ni, (c) WS_2/Cr, and (d) WSe_2/Ni were calculated for three different topologies using the extended Hückel semiempirical method. Enhanced PDOS values near the Fermi level are observed in the chalcogen interstitial contact topology, hence making this contact topology intriguing for further investigations.

that having a chalcogen atom at an interstitial site on the TMD surface results in significant spread in the transmission coefficient and DOS across a wider range of energy levels. Qualitatively, it reveals enhanced carrier injection through contacts with the chalcogen atom at the interstitial site. The effect of chalcogen atom on the interface is quantified through contact current calculations that directly are related to contact resistance. Fig. 5 shows the lower interface resistance with the introduction of chalcogen atom at the TMD–metal interface. These computational findings predict the possibility of contact improvement with chalcogen treatment over the TMD surface.

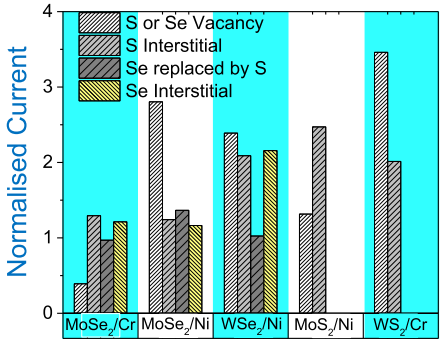

Fig. 5. Current across different TMD/metal contacts with all possible contact topologies involving chalcogen atoms, normalized with current across standard contact. Current across the contact has a direct relation with contact resistance. Therefore, higher current implies lower contact resistance (R_C) in the case of chalcogen interstitial contact topologies than in the case of standard contact. Physical understanding of mechanism behind lower contact resistance in chalcogen interstitial should help in engineering the contacts at 2-D TMD/metal interfaces.

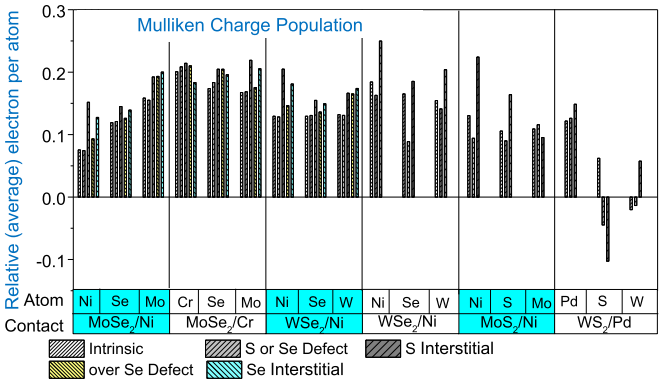

Fig. 6. MCP extracted for all the contact topologies discussed earlier. Shift in the electron cloud toward the interface atomic species is predicted from MCP.

Furthermore, Mulliken charge population (MCP) is extracted for the constituent atoms to understand how the metal–TMD interface is altered after introducing the chalcogen atom at various TMD–metal interfaces, as depicted in Fig. 6. It is observed that for all the TMD–metal interfaces, the amount of average charge shared in the contact region (i.e., at the interface) by all the constituent atoms has increased from its reference value in the noncontacted bulk crystals. This increase is found to be highest for the topology with chalcogen interstitial. The observation of lower contact resistance with increased charge share across atomic species at the interface implies enhanced orbital interaction between the metal and the TMD, which resulted in improved bonding and contact property. It is worth highlighting that the source of such an increase in the charge around all atomic species at the interface must be the semiconductor bulk and not the introduced chalcogen atom. This can be visualized as higher electron density/concentration at the contact region, which classically can be considered as the doping of the semiconductor crystal at the metal–TMD interface. The effect of such a chalcogen-assisted self-doping of the TMD–metal interface on its interface properties is expected to be unique for different contact metals depending on the available overlapping atomic orbitals for interaction or hybridization.

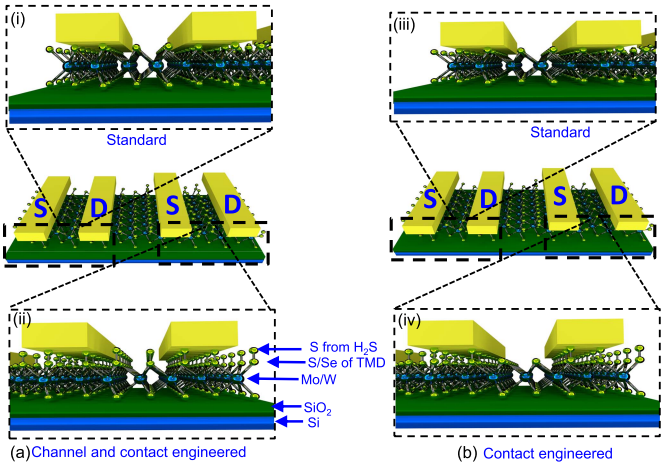

Fig. 7. Scheme representing fabricated (a) standard contact- and channel-engineered and (b) standard and contact-engineered transistors on the same TMD flake. Yellow spheres represent chalcogen atoms (sulfur and/or selenium), whereas blue spheres represent the transition metal atom (molybdenum and tungsten).

IV. Experimental Framework

Based on computational finding, now, the problem statement is to introduce the chalcogen atom at the TMD–metal interface. H_2S is a widely used sulfur source for the CVD growth of S-based TMDs, which partially decomposes at lower temperatures in the presence of TMDs. In the presence of the TMDs, besides satisfying S vacancies, H_2S also tends to get adsorbed at the TMD surface, thereby forming the S–S (S–Se) bond between S from H_2S and S (Se) bonded to an adjacent Mo/W atom in the TMD, as depicted in Fig. 7. Typically, complete decomposition of H_2S requires higher temperatures; however, the presence of a TMD surface catalyzes the decomposition reaction and H_2S breaks into S. Here, S stays bonded with the S/Se atom at the TMD surface and H_2 leaves the surface after initial adsorption, as discussed above. In order to release S from the surface of the TMD, another catalytic reaction is carried out, which ensures complete low-temperature decomposition of H_2S into S and H_2. This decomposition process was earlier validated by work in [22]. In this article, we perform only the first step of complete decomposition of H_2S i.e., bonding of S on the TMD surface followed by the release of H_2. Subsequent step to catalyze the release of S is avoided intentionally so that a contact topology with S interstitial can be achieved. To uniformly introduce S doping over TMD top layer, TMD samples were treated with H_2S inside a quartz tube at 350 °C while varying the H_2S partial pressure. The resultant device variants are depicted in Fig. 7. To develop the standard and engineered devices, as depicted in Fig. 7, the following process was adopted: synthesized TMD crystals from 2-D Semiconductors were exfoliated using the Scotch tape method and transferred over a (Piranha and Acetone/IPA cleaned) 90-nm SiO_2 on the heavily doped p-type Si substrate from NOVA wafers. Few layered flakes were identified using an optical microscope followed by alignment marks patterning and deposition. After precise determination of the flakes, the sample was spin-coated with bilayer PMMA (495 A4 at 3000 r/min/950 A2 at 3000 r/min) using a spin coater.

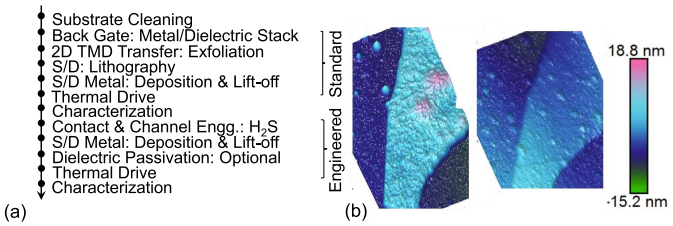

Fig. 8. (a) Fabrication process flow for standard and engineered devices. (b) AFM image of the MoS_2 flake (left) before and (right) after the H_2S-based atomic orbital overlap engineering clearly depicts significant reduction in rms surface roughness and removal of residues from the top.

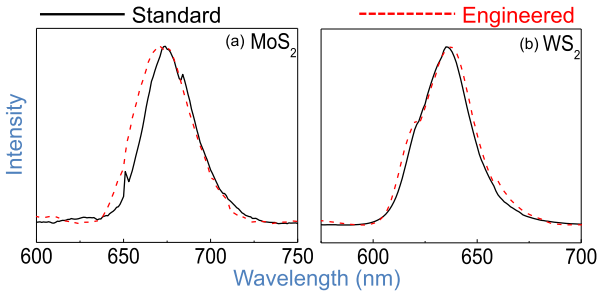

Fig. 9. PL spectra of (a) MoS_2 and (b) WS_2 before and after H_2S treatment. The peaks corresponding to direct bandgap (675 nm/1.8 eV for MoS_2 and 640 nm/1.94 eV for WS_2) do not show significant shift in frequency, which confirms no change in the direct bandgap of the material. This shows that the material was conserved without a noticeable change in its semiconducting properties.

Source and drain contact pads were patterned using e-beam lithography, across one-half of the flake, followed by development in 1:3/MIBK:IPA. Contact metal was then deposited inside an e-beam evaporator (TECPORT) under pressure as low as 10^{-6} torr followed by metal liftoff. Post liftoff, annealing was done at 200 °C for 10 min. After electrically characterizing these devices, the same flakes were treated using H_2S (as discussed in the previous section). Posttreatment, the H_2S-treated region of the flake (which is the other half of the flake) was used to fabricate a back-gated FET, which is called the as-treated or engineered device. The fabrication process followed here was the same as that for the nontreated device on the other half of the flake, and process flow is shown in Fig. 8(a). It should be noted that for one to one comparison, standard and engineered device was fabricated over the same flake, side by side. Samples were characterized using AFM, photoluminescence, Raman spectroscopy, and XPS before and after H_2S treatment. An AFM surface map of MoS_2, as depicted in Fig. 8(b), reveals that H_2S treatment leads to a smoother surface by curing surface defects present on an otherwise-untreated TMD surface. Furthermore, PL spectra shown in Fig. 9 show that the material properties in terms of bandgap and semiconducting nature remain unchanged post-H_2S treatment. Raman spectra depicted in Fig. 10 reveal two peaks: E_{2g} and A_{1g}, which correspond to in-plane and out-of-plane phonon modes, respectively, which are present before and after H_2S exposure. This confirms that the fundamental molecular structure of the TMD remains intact posttreatment. Post-H_2S exposure, a blue shift in A_{1g} peak is observed,

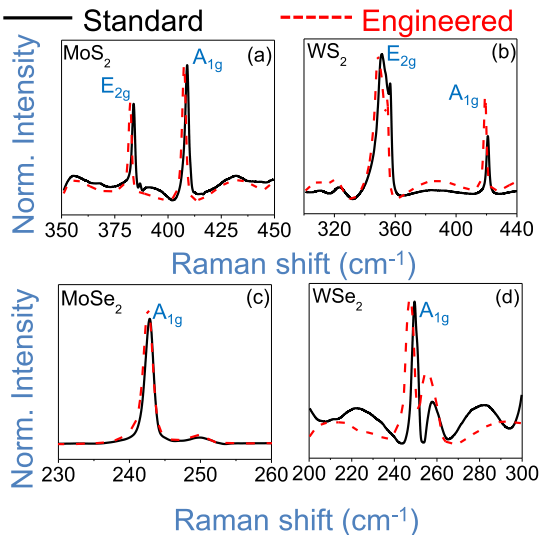

Fig. 10. (a)–(d) Raman spectra of as-exfoliated and engineered (H_2S-treated) MoS_2, WS_2, $MoSe_2$, and WSe_2 flakes. Narrowing of the Raman peaks along with the lowering of shoulders close to peaks depicts satisfaction of sulfur vacancies. A red shift is consistently observed for all TMDs, implying increased electron–phonon coupling. This observation validates the anticipated (from MCP calculations) shift in the electron cloud toward the surface from bulk after H_2S exposure.

which is attributed to increased electron phonon interaction at the TMD surface [23]. This is due to the shift in the electron cloud toward the surface in the presence of added S atoms. It should be noted, however, that, since S is a highly electronegative atom, this electron cloud is confined to the S atoms. This also results in a positive shift in V_{TH}, which will be disclosed in the subsequent sections. Raman spectra further show lower full-width half-maximum (FWHM) after treatment, which signifies lesser defects in the treated sample. It should be noted that most of the defects in TMDs are chalcogen vacancies on the surface, which were found to have reduced post-H_2S treatment. The same is further validated using XPS, as depicted in Fig. 11(a) and (b). Here, Mo:3d3/2, Mo:3d5/2, and S:2s have resulted from the reduction of +5 and +6 oxidation states of Mo, which reveals relatively lower number of sulfur vacancies in the treated samples. The same defect mitigation can be seen for W 4f and 5p states in WS_2 from Fig. 11(c). As shown in Fig. 11(a) and (b), additional S peaks are obtained, which could be a result of S–S or Se–S bonds at the surface of TMDs and(or) S–Mo bonds on the surface of $MoSe_2$, which were absent in an otherwise-pristine $MoSe_2$ surface. In summary, AFM (see Fig. 8), PL (see Fig. 9), Raman (see Fig. 10), and XPS (see Fig. 11) spectra captured before and after H_2S-assisted surface engineering confirm: 1) increase in the electron (bonded to S) concentration at the surface of TMD; 2) passivation of S-vacancies; and 3) presence of S–S (S–Se) bonds in S (Se)-based TMDs when treated with H_2S.

V. Experimental Validation and Results

Implications of such a treatment on the device thereby engineering the contact and channel regions to realize the desired device behavior are studied by fabricating backgated TMD FETs. In order to capture the effect of H_2S treatment on contact as well as channel, devices were exposed to H_2S in the: 1) contact region and 2) channel as well as contact region, as shown in Fig. 7. A flow that allows to independently quantifying the effect of chalcogen-based engineering over the channel and the contact was adopted. Contact-engineered MoS_2 and WS_2 FETs exhibit 3× and 5× higher ON current, respectively, without affecting OFF-state current and threshold voltage when compared with standard FETs [see Fig. 12(a) and (b)]. On the other hand, the ON- and OFF-state performances of the contact-engineered $MoSe_2$ FETs have been improved by 2× and five orders, respectively [see Fig. 12(c)]. Improved ON-state current is a result of S-assisted charge sharing at the TMD–metal interface. The OFF-state performance of the contact-engineered MoS_2 and WS_2 FETs is unaffected by H_2S exposure, as the channel was masked against H_2S treatment, thereby retaining its intrinsic channel properties. However, H_2S-assisted contact engineering on $MoSe_2$ FET led to a complete device turn OFF at $V_{GS} = -20$ V, which was otherwise ON at the same V_{GS}. Such a drastic reduction in the OFF-state current and enhancement-mode operation is explained to be an effect of stronger interaction between the S interstitial atom and the electrons in its vicinity that keeps the device turned OFF until a relatively higher V_{GS}, when compared with the device without treatment. This interaction is relatively weak in MoS_2 and WS_2 FETs compared with that in $MoSe_2$ due to the difference in the atomic orbitals involved in the Se-based TMDs when compared with the S-based TMDs. This can be explained as follows: S is more electronegative than Se. This is because of the size and the 2p orbital in the outermost shells of S, unlike Se that has 3p and 3d orbitals in the outermost shell(s). Hence, S tends to have stronger Coulombic interaction with electrons than Se. When a S atom is added on a Se-based TMD surface, the electron cloud will experience stronger Coulombic interaction from the S atom than the case where S is added on the surface of a S-based TMD. Therefore, in a Se-based TMD, the effect of S addition is expected to be stronger than the addition of S in a S-based TMD. Contact with channel-engineered MoS_2 and WS_2 FETs exhibit 71× and 86× improvement in ON-state performance and two- and one-order reductions in OFF-state leakage, respectively. Moreover, $MoSe_2$ FETs confirm to have large positive V_{TH}, and therefore exhibit three orders of magnitude lower OFF-state current than the standard FETs [see Fig. 12(d)–(f)].

A. Overall Performance Boost

Typical doping techniques reported elsewhere result in increased leakage current and suppressed gate control. In this article, however, leakage current has reduced by a significant amount, leading to higher current modulation along with improved gate control as well as other performance metrics in treated FETs. In general, for all TMDs, contact engineering with H_2S leads to improved contact performance and proposed channel engineering offers an improved OFF-state behavior besides improved gate control. Such a unique improvement in the overall device performance has been demonstrated for the first time. It should, however, be noted that the magnitude of improvement depends on TMD material and contact metal.

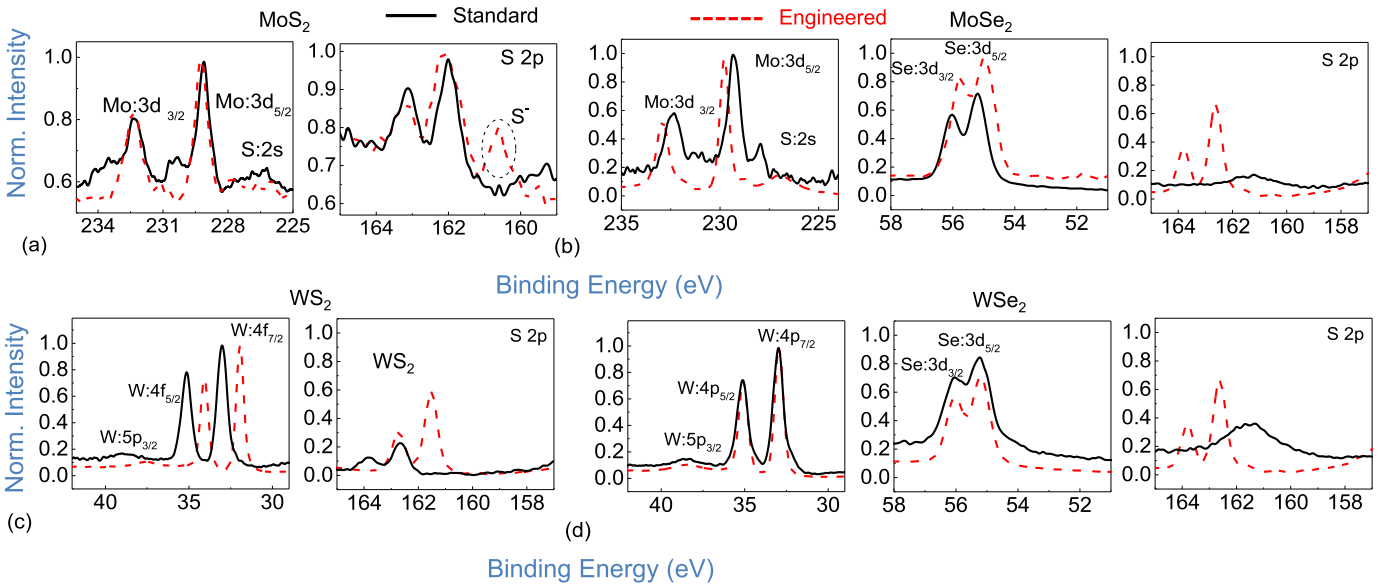

Fig. 11. XPS spectra for (a) MoS_2, (b) $MoSe_2$, (c) WS_2, and (d) WSe_2 samples before and after H_2S exposure show reduced shoulders near the 3d peaks of Mo, which imply that reduction in S vacancy/defects and Mo dangling bonds presents in the material. This validates the theory of defect curing. Presence of S in the engineered $MoSe_2$ surface reveals that H_2S exposure is a reliable method to introduce S atoms at the surface to enable the unique charge distribution mechanism and atomic orbital overlap at the interface.

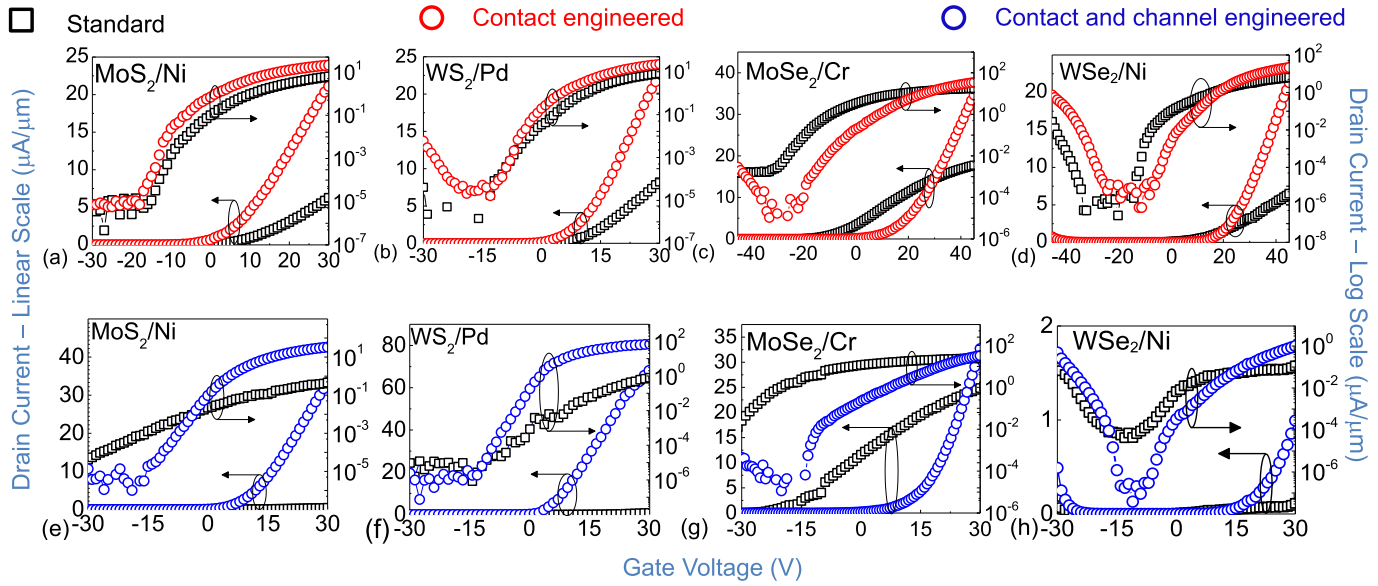

Fig. 12. (a)–(d) Contact-engineered MoS_2, WS_2, $MoSe_2$, and WSe_2 FETs ($L_{CH} = 1\ \mu m$, $V_{DS} = 1$ V, and gate dielectric = 90 nm, SiO_2). (e)–(h) Channel with contact-engineered MoS_2, WS_2, $MoSe_2$, and WSe_2 FETs ($L_{CH} = 1\ \mu m$, $V_{DS} = 1$ V, and gate dielectric = 90 nm, SiO_2).

Fig. 13 summarizes the overall performance improvement in terms of various figure-of-merit parameters (I_{ON}, g_m, μ, I_{OFF}, SS, I_{ON}/I_{OFF}, and R_C) by using the proposed contact and channel-engineering technique. Significantly improved mobility, R_C, and transconductance are the results of transparent contact and improved channel properties. It is worth mentioning that contact resistance is extracted using the Y-function technique. Although the extracted values of R_C from the Y-function method are usually not reliable, it is important to emphasize on the relative improvement in the contact resistance for all the devices after H_2S-assisted contact and channel engineering. Fig. 14 shows the contact resistance extracted from the Y-function method for MoS_2 and WS_2 FETs as a function of gate voltage. To extract contact resistance, the following formula was used: $R_C = {s_1}^{-1}\ s_2\ V_d$, where, s_1 = Slope $(1/\sqrt{g_m})$; s_2 = Slope (Y, V_g), and $Y = I_d/\sqrt{g_m}$ [24].

In order to probe the effect of this treatment on the metal–TMD interface, Schottky barrier height (SBH) is extracted using the thermionic emission theory [25]. It is found that SBH for WS_2/Pd after treatment is negative (−20 meV) unlike the SBH (46 meV) before treatment, which is positive. Negative SBH implies an ohmic contact [22]. Stronger Fermi-level pinning, after H_2S exposure, is expected due to

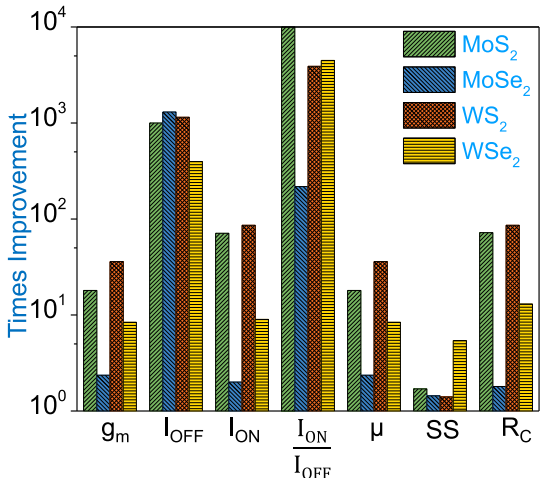

Fig. 13. Improvement in the performance figure-of-merit parameters for various TMD FETs while using proposed contact or/and channel engineering.

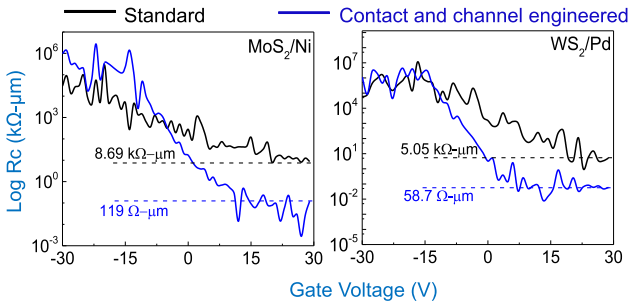

Fig. 14. Improvement in contact resistance of MoS_2 and WS_2 FETs after H_2S treatment.

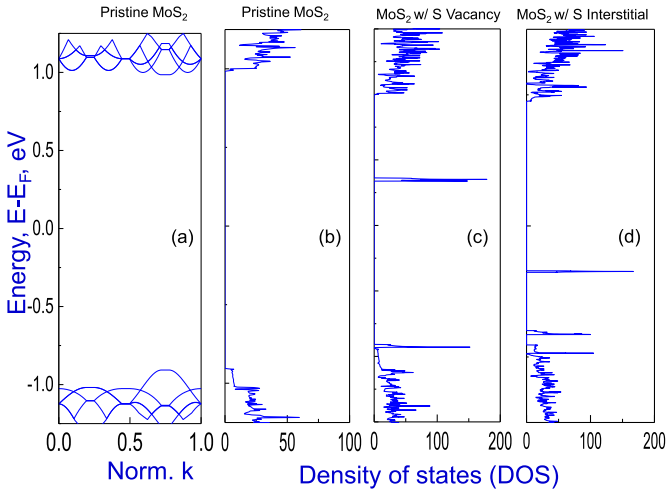

Fig. 15. (a) Band structure of monolayer MoS_2, exhibiting a direct bandgap. (b) DOS in a defectless MoS_2 monolayer. Absence of energy states within the bandgap can be observed. (c) DOS in a monolayer MoS_2 with S vacancy. The presence of donor-type surface states within the bandgap is observed. (d) DOS in a monolayer MoS_2 with an S interstitial atom. Here, K point path is G (o) (k=0) → M (k=0.194) → L (k=0.248) → A (kX0.443) → G (o) (k=0.497) → K (k=0.721) → H (k=0.775) → A (k=1).

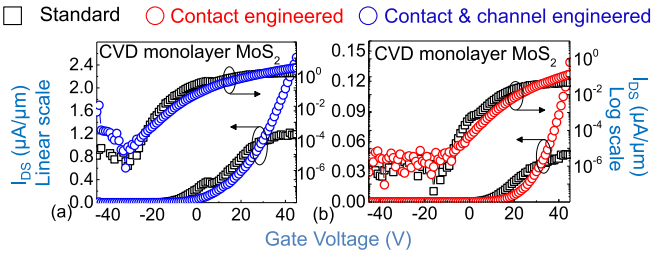

Fig. 16. (a) and (b) CVD monolayer MoS_2 FETs exhibit enhanced performance after H_2S exposure for contact and contact with channel engineering, respectively. Defect-limited transport is enhanced by curing the defects present in CVD MoS_2 via channel with contact engineering while enhancing current injection through contacts (L_{CH} = 1 μm, V_{DS} = 4 V, and SiO_2 90 nm).

the increase in the number of surface states [26]. Increase in the number of surface states is attributed to the presence of more acceptor-like states within the bandgap as a result of the formation of S–S bonds after the treatment. The presence of acceptor-like states on the TMD surface is confirmed using atomistic simulations, as shown in Fig. 15. DOS of three types of monolayer MoS_2 structures— defectless structure, with S vacancies, and with S atom as interstitial—is calculated. Defectless crystal does not have any states in the bandgap unlike other two structures, where surface states appear within the bandgap. For MoS_2 with S vacancy, surface states lie near the conduction band minimum, while for MoS_2 with S interstitial, surface states have surface states near the valence band maximum. It is expected that the presence of large number of surface states near the valence band results in the lowering of charge neutrality level (CNL) of the semiconductor and subsequent pinning of the Fermi level at lower energy such that an ohmic contact is formed.

B. Monolayer CVD TMD

Physical insights into the unique charge sharing mechanism and its experimental validation encouraged positive implications of this process on the CVD TMD monolayer so that its technological relevance can be unveiled (see Fig. 16). The ON-state performance of the CVD monolayer MoS_2 FETs was found to improve by 4× and 3× for the contact and the contact with the channel-engineered FETs, respectively. In addition, the OFF-state leakage remains unchanged for both the types of engineered devices. Standard CVD monolayer MoS_2 FETs are limited in terms of performance due to high defect density (manifests as plateau in transfer characteristics; see Fig. 16) and high contact resistance due to large bandgap. Disappearance of the plateau in the transfer curve further confirms the elimination of defect states because of proposed channel engineering. Finally, a noticeable shift in threshold voltage was observed, leading to the first demonstration of enhancement-mode CVD MoS_2 FETs. This is also attributed to reduction in S vacancies after the channel treatment/curing of intrinsically defected CVD TMD material. This treatment has led to a significant improvement in all the device parameters of TMD-based FETs. When compared with other devices in the literature, H_2S-treated devices—as proposed in this article—exhibit comparable or better performance than the best number reported in literature. This is shown in Fig. 17.

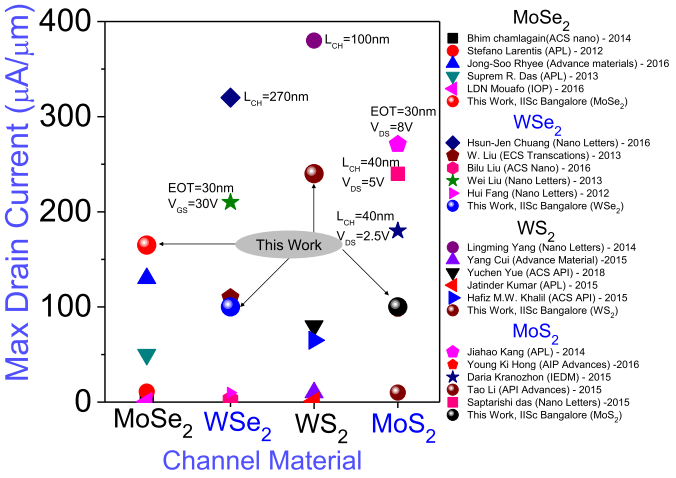

Fig. 17. ON current comparison with the state-of-the-art 2-D TMD FETs. ON-current in this article was extracted for $V_{GS} = 30$V, $V_{DS} = 4$ V, $L_{CH} = 1$ μm, and EOT = 90 nm.

VI. Conclusion

Developed physical understanding of unique atomic orbital interaction among TMDs, chalcogen atoms, and metals, a scalable approach to engineer the TMD/metal interface and the TMD channel has been proposed and experimentally demonstrated for four different TMD materials (MoS_2, WS_2, $MoSe_2$, and WSe_2). S-assisted enhanced orbital interaction at the TMD/metal interface resulted in transparent contacts, which led to reduced metal–TMD contact resistance and improved ON-state performance. On the other hand, S-assisted channel engineering, attributed to the annihilation of intrinsic defects in the TMD channel, has improved the OFF-state behavior and led to a controlled transition from depletion-mode operation to the enhancement-mode operation of the 2-D FETs. Detailed understanding of the quantum chemistry involved has eased the generality of this process over S- and Se-based TMDs. The proposed method universally results in a significant improvement in the channel and contact performances, thereby improving the overall transistor behavior, for the entire range of the experimented 2-D TMDs. Finally, technological relevance of the proposed scheme has been validated for the monolayer CVD material.

References

[1] M. Shrivastava *et al.*, "Toward system on chip (SoC) development using FinFET technology: Challenges, solutions, process co-development & optimization guidelines," *IEEE Trans. Electron Devices*, vol. 58, no. 6, pp. 1597–1607, Jun. 2011, doi: 10.1109/TED.2011.2123100.

[2] M. Shrivastava *et al.*, "Benchmarking the device performance at sub 22 nm node technologies using an SoC framework," in *IEDM Tech. Dig.*, Dec. 2009, pp. 1–4, doi: 10.1109/IEDM.2009.5424311.

[3] K. Hemanjaneyulu and M. Shrivastava, "Fin enabled area scaled tunnel FET," *IEEE Trans. Electron Devices*, vol. 62, no. 10, pp. 3184–3191, Oct. 2015, doi: 10.1109/TED.2015.2469678.

[4] A. Rajoriya, M. Shrivastava, H. Gossner, T. Schulz, and V. R. Rao, "Sub 0.5 V operation of performance driven mobile systems based on area scaled tunnel FET devices," *IEEE Trans. Electron Devices*, vol. 60, no. 8, pp. 2626–2633, Aug. 2013, doi: 10.1109/TED.2013.2270566.

[5] B. Radisavljevic, A. Radenovic, J. Brivio, V. Giacometti, and A. Kis, "Single-layer MoS_2 transistors," *Nature Nanotechnol.*, vol. 6, p. 147, Jan. 2011, doi: 10.1038/nnano.2010.279.

[6] A. Nourbakhsh *et al.*, "MoS_2 field-effect transistor with sub-10 nm channel length," *Nano Lett.*, vol. 16, no. 12, pp. 7798–7806, Dec. 2016, doi: 10.1021/acs.nanolett.6b03999.

[7] S. Larentis, B. Fallahazad, and E. Tutuc, "Field-effect transistors and intrinsic mobility in ultra-thin $MoSe_2$ layers," *Appl. Phys. Lett.*, vol. 101, no. 22, 2012, Art. no. 223104.

[8] J.-S. Rhyee *et al.*, "High-mobility transistors based on large-area and highly crystalline CVD-grown $MoSe_2$ films on insulating substrates," *Adv. Mater.*, vol. 28, no. 12, pp. 2316–2321, Mar. 2016, doi: 10.1002/adma.201504789.

[9] D. Ovchinnikov, A. Allain, Y.-S. Huang, D. Dumcenco, and A. Kis, "Electrical transport properties of single-layer WS_2," *ACS Nano*, vol. 8, no. 8, pp. 8174–8181, Aug. 2014, doi: 10.1021/nn502362b.

[10] J. Kumar, M. A. Kuroda, M. Z. Bellus, S.-J. Han, and H.-Y. Chiu, "Full-range electrical characteristics of WS_2 transistors," *Appl. Phys. Lett.*, vol. 106, no. 12, Mar. 2015, Art. no. 123508, doi: 10.1063/1.4916403.

[11] S. Das and J. Appenzeller, "WSe_2 field effect transistors with enhanced ambipolar characteristics," *Appl. Phys. Lett.*, vol. 103, no. 10, Sep. 2013, Art. no. 103501, doi: 10.1063/1.4820408.

[12] W. Liu, J. Kang, D. Sarkar, Y. Khatami, D. Jena, and K. Banerjee, "Role of metal contacts in designing high-performance monolayer n-type WSe_2 field effect transistors," *Nano Lett.*, vol. 13, no. 5, pp. 1983–1990, May 2013, doi: 10.1021/nl304777e.

[13] H. Fang *et al.*, "Degenerate n-doping of few-layer transition metal dichalcogenides by potassium," *Nano Lett.*, vol. 13, no. 5, pp. 1991–1995, May 2013, doi: 10.1021/nl400044m.

[14] Y. Du, H. Liu, A. T. Neal, M. Si, and P. D. Ye, "Molecular doping of multilayer MoS_2 field-effect transistors: Reduction in sheet and contact resistances," *IEEE Electron Device Lett.*, vol. 34, no. 10, pp. 1328–1330, Oct. 2013, doi: 10.1109/LED.2013.2277311.

[15] L. Yang *et al.*, "Chloride molecular doping technique on 2D materials: WS_2 and MoS_2," *Nano Lett.*, vol. 14, no. 11, pp. 6275–6280, Nov. 2014, doi: 10.1021/nl502603d.

[16] D. Kiriya, M. Tosun, P. Zhao, J. S. Kang, and A. Javey, "Air-stable surface charge transfer doping of MoS_2 by benzyl viologen," *J. Amer. Chem. Soc.*, vol. 136, no. 22, pp. 7853–7856, Jun. 2014, doi: 10.1021/ja5033327.

[17] G. P. Neupane *et al.*, "Simple chemical treatment to n-dope transition-metal dichalcogenides and enhance the optical and electrical characteristics," *ACS Appl. Mater. Interfaces*, vol. 9, no. 13, pp. 11950–11958, Apr. 2017, doi: 10.1021/acsami.6b15239.

[18] S. Mouri, Y. Miyauchi, and K. Matsuda, "Tunable photoluminescence of monolayer MoS_2 via chemical doping," *Nano Lett.*, vol. 13, no. 12, pp. 5944–5948, Dec. 2013, doi: 10.1021/nl403036h.

[19] K. Hemanjaneyulu, J. Kumar, and M. Shrivastava, "MoS_2 doping using potassium iodide for reliable contacts and efficient FET operation," *IEEE Trans. Electron Devices*, vol. 66, no. 7, pp. 3224–3228, Jul. 2019.

[20] R. Kappera *et al.*, "Phase-engineered low-resistance contacts for ultra-thin MoS_2 transistors," *Nature Mater.*, vol. 13, p. 1128, Aug. 2014, doi: 10.1038/nmat4080.

[21] S. Das, H.-Y. Chen, A. V. Penumatcha, and J. Appenzeller, "High performance multilayer MoS_2 transistors with scandium contacts," *Nano Lett.*, vol. 13, no. 1, pp. 100–105, Jan. 2013.

[22] A. N. Startsev *et al.*, "Low-temperature catalytic decomposition of hydrogen sulfide on metal catalysts under layer of solvent," *J. Sulfur Chem.*, vol. 37, no. 2, pp. 229–240, Mar. 2016, doi: 10.1080/17415993.2015.1126593.

[23] B. Chakraborty, A. Bera, D. V. S. Muthu, S. Bhowmick, U. V. Waghmare, and A. K. Sood, "Symmetry-dependent phonon renormalization in monolayer MoS_2 transistor," *Phys. Rev. B, Condens. Matter*, vol. 85, no. 16, Apr. 2012, Art. no. 161403, doi: 10.1103/PhysRevB.85.161403.

[24] C. Liu, Y. Xu, and Y.-Y. Noh, "Contact engineering in organic field-effect transistors," *Mater. Today*, vol. 18, no. 2, pp. 79–96, 2015. [Online]. Available: http://www.sciencedirect.com/science/article/pii/S1369702114003204

[25] D. Qiu and E. K. Kim, "Electrically tunable and negative Schottky barriers in multi-layered graphene/MoS_2 heterostructured transistors," *Sci. Rep.*, vol. 5, Sep. 2015, Art. no. 13743, doi: 10.1038/srep13743.

[26] C. Gong, L. Colombo, R. M. Wallace, and K. Cho, "The unusual mechanism of partial Fermi level pinning at metal-MoS_2 interfaces," *Nano Lett.*, vol. 14, no. 4, pp. 1714–1720, Apr. 2014, doi: 10.1021/nl403465v.